Journal of Materials Chemistry A

Accepted Manuscript

This is an *Accepted Manuscript*, which has been through the Royal Society of Chemistry peer review process and has been accepted for publication.

Accepted Manuscripts are published online shortly after acceptance, before technical editing, formatting and proof reading. Using this free service, authors can make their results available to the community, in citable form, before we publish the edited article. We will replace this *Accepted Manuscript* with the edited and formatted *Advance Article* as soon as it is available.

You can find more information about *Accepted Manuscripts* in the Information for Authors.

Please note that technical editing may introduce minor changes to the text and/or graphics, which may alter content. The journal's standard Terms & Conditions and the Ethical guidelines still apply. In no event shall the Royal Society of Chemistry be held responsible for any errors or omissions in this *Accepted Manuscript* or any consequences arising from the use of any information it contains.

ROYAL SOCIETY OF CHEMISTRY

www.rsc.org/materialsA

Journal Name

ARTICLE

Nitrogen-doped Porous Carbon Derived from Residuary Shaddock Peels: A Promising and Sustainable Anode for High Energy Density Asymmetric Supercapacitors†

Received 00th January 20xx,
Accepted 00th January 20xx

DOI: 10.1039/x0xx00000x

www.rsc.org/

Kang Xiao,[a] Liang-Xin Ding,*[a] Hongbin Chen,[a] Suqing Wang,[a] Xihong Lu[b] and Haihui Wang*[a]

Exploring high-performance negative electrode material is one of great challenges in the development of high-energy density asymmetric supercapacitors (ASCs). Herein, a new kind of high-performance nitrogen-doped nanoporous carbon (NPC) electrode with large surface area and abundant micropores/mesoporous was derived from a conveniently available fruits waste (shaddock peels) via a facile pyrolysis process. Electrochemical measurements show that the as-synthesized NPC electrodes possessed a remarkably large capacitance of 321.7 F g^{-1} with good rate capability and excellent long-term cycling stability. Such the excellent electrochemical performance was achieved by shortening the diffusion distance, increasing electrode-electrolyte contact area and improving the electron conductivity of NPC electrode arising from its nanoporous architecture and nitrogen doping. As a prototype, an all-solid-state ASC device based on the NPC negative electrode and a MnO_2 positive electrode achieved an ultrahigh energy density of 82.1 W h Kg^{-1} at a power density of 899 W Kg^{-1}, which is considerably larger than most of the reported carbon based supercapacitor devices.

Introduction

Along with increased concern over the power and energy demand for next-generation energy storage devices, supercapacitors (SCs) have attracted a great deal of attention as a priority candidate of future renewable energy storage for hybrid electric vehicles, and other high power applications due to their long life cycle, high specific power density and highly reversible charge storage process. However, the energy density of SCs is still relatively low, which is seriously impede their application in future.[1] In comparison to conventional SCs, constructing asymmetric supercapacitors (ASCs) are regarded as an effective approach to increase the energy density which can make full use of different potential windows of the positive and negative electrode to increase the cell voltage, resulting in higher energy density than symmetry supercapacitors (SSCs).[2] However, for one entire cell, the overall capacitance C_t is mainly dominated by the one with smaller according to the equation ($C_t^{-1} = C_p^{-1} + C_n^{-1}$). So far, various high performance pseudocapacitive cathode electrodes materials have been investigated in ASCs such as transition metal oxides/hydroxide [3] and conducting polymer,[4] but high-performance negative electrodes are relatively less involved. Carbon materials such as grapheme,[1d,5] carbon nanotubes [6] and activated carbon [3b,7] with good electronic conductivity, excellent electrochemical stability and large surface area have been commonly used as negative electrodes for ASCs. Unfortunately, these conventional carbon materials are not yet satisfactory for ASCs anode because the low specific capacitance (< 200 F g^{-1}) severely limits the overall capacitance of ASCs.[8] Therefore, to meet the demands for high energy density devices, the capacitance of carbon materials must boosted further. Moreover, most of carbon materials are derived from non-renewable petroleum-based chemical products,[7] which is introduces the high cost because of the fossil fuel and environmental crisis looming in the near future.

Recently, carbon materials derived from biomass waste such as Banana peels, Peanut shell, Bamboo chopsticks, Typha orientalis, Cotton, olive pit, corn cob, et al.[9] have been received extensively attention because of their fascinating structure and wide applications in oxygen reduction reaction, Li-ion battery, Na-ion battery and SCs. For example, Fan et al. [10] reported a kind of densely porous graphene-like carbon (PEC) through hydrothermal treatment and subsequent carbonization of fungus. The PGC electrode exhibited a high specific capacitance of 374 F g^{-1} at a current density of 0.5 A g^{-1}. Cao et al.[11] fabricated micro/mesopores interconnected structures of 3D carbon with high specific surface areas (2475 m^2 m^{-1}) through carbonization and activation of rice brans. The maximum specific capacitance of 621.6 F g^{-1} has been obtained at a current density of 1 A g^{-1}. Additionally, recent report has shown that incorporation of heteroatoms could significantly improve the surface hydrophilicity and conductivity of carbon materials resulting higher specific capacitance and rate capability. For instance, Cao et al.[12] reported hierarchical porous nitrogen-doped carbon prepared though activation and graphitization of natural silk in N_2 presented an improved capacitance (242 F g^{-1} at 0.1 A g^{-1}) and rate performance (213 and 155 F g^{-1} at a high current

[a] School of Chemistry & Chemical Engineering, South China University of Technology, No. 381 Wushan Road, Guangzhou 510640, China. E-mail: lxding@scut.edu.cn; hhwang@scut.edu.cn
[b] School of Chemistry and Chemical Engineering, Sun Yat-Sen University, Guangzhou 510275, China

† Electronic Supplementary Information (ESI) available: Experimental details and results for all reported experiments. See DOI: 10.1039/x0xx00000x

Journal of Materials Chemistry A Accepted Manuscript

density of 1 and 10 A g^{-1}). However, two challenges remain. First, the majority of hierarchically porous carbons derived from natural bio-material need to chemical activation process with alkali to create meso- and macro-porous structure, which is complicated for practical application. Another disadvantage is that using ammonia/nitrogen gas as the N source is difficult to form uniform nitrogen doping.

In this work, we reported a new kind of nitrogen-doped nanoporous carbon (NPC) derived from shaddock peels without template or pretreatment process as an advanced negative electrode for high energy density ASCs. Shaddock is one kind of commonly eaten fruit in China and Southeast Asia countries. Most of shaddock peels are usually treated as a kind of agricultural waste and directly discarded in the garbage dump, which is harmful for environment when they decay. Actually, the white flocculent layer in shaddock peels consisting of many small cellulose fibers is an ideal carbon precursor to produce natural porous carbon fibers. Moreover, the spongy-like shaddock peels has a strong solution absorption capacity toward metallic and organic solution, which provides an excellent platform for further optimizing its structure and property. Herein, we developed a template-free and smart strategy to prepare NPC materials with high surface area and porosity by a facile soak process in melamine solution and post-treatment in Ar. Such a unique N-doped porous carbon can deliver a high specific capacity of 321.7 F g^{-1} at a current density of 1 A g^{-1} and excellent cycling ability. When used as negative electrode for ASCs, a high-performance all solid-state MnO_2//NPC-ASC device with a high energy density of 82.1 KW Kg^{-1} has been achieved.

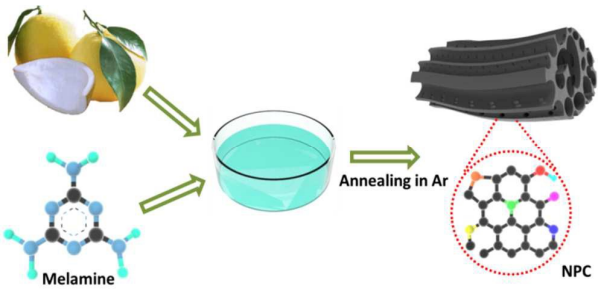

Fig. 1 Schematic illustration for the formation of nitrogen-doped porous carbon.

Results and discussion

Fig. 1 illustrates the synthetic process of the NPC electrodes. Firstly, the dried shaddock peels were soaked in a saturated melamine solution for 10 min. Scanning electron microscopy (SEM) images (Fig. S1) reveal that the dried shaddock peels have a continuous 3D fibrous structure with pore size ranging from 100 to 200 μm, which is in favour of melamine adsorption. Secondly, to obtain the NPC, the shaddock peels contain with melamine were carbonized at 600-900 ^{o}C for 4 h (see ESI for details).

X-ray diffraction (XRD) patterns of the NPCs samples carbonized at different temperatures were collected in Fig. 2a. All of these NPC materials possess two broad peaks located at around 26° and 44°, corresponding to the 002 and 100 planes of the typical turbostratic carbon, which demonstrates the presence of graphitic carbon.[13] Particularly, the intensity of the peak increased with the increased annealing temperature indicates that high temperature is benefit for graphitization, which is also confirmed by Raman spectra analysis (Fig. 2b). The peaks located at 1350 cm^{-1} (D band) and 1590 cm^{-1} (G band) correspond to the defects and graphitic carbon, respectively.[9e-d] The intensity ratio of I_G/I_D is summarized in Fig. S2. The I_G/I_D ratio is obviously increases from 0.63 for NPC-600 to 0.88 for NPC-900, showing the NPC-900 has the best graphitization. Fig. 2(c-d) shows the representative SEM images of the NPC-700. The 3D scaffold with a fold surface structure was retained after carbonization process. It is interesting that such a fiber was consist of several hollow tubes with a diameter of 2-10 μm and a continuous porous network are observed at the hollow tubes wall, forming a 3D ordered porous structure. The element mappings clearly revealed that the product contains uniform C, N and O elements (Fig. S3). The SEM images of NPC-600, NPC-800 and NPC-900 show that the morphology has no obvious change with the different carbonization temperature, and the plenty of nanosized holes was interconnected neighboring hollow tube each other (Fig. S4).

In order to investigate the detailed microstructure of the samples, TEM and high-resolution TEM (HRTEM) were carried out. Fig. 2e presents the HRTEM of NPC-700, which clearly reveals that the samples are made up of many micropores and channels (white spots in gray areas) with 2D layered structure, which results in a high surface area. The selected area electron diffraction (SAED) pattern of NPC-700 (Fig. 2e inset) demonstrated the formation of graphitized carbon. In addition, the lattice fringes of carbon layers (Fig. S5) was increasing with the carbonization temperature, indicating the formation of graphitic carbon. The HRTEM micrographs were also agreeing with the XRD and the Raman results.

To further confirm the percentage of N-incorporation and the elemental composition, the samples were examined by XPS. According to the XPS results, C 1s, O 1s and N 1s can be observed in the survey XPS spectra (Fig. S6a) and no obvious N 1s signal was found in the untreated PC samples, indicating the NPC samples were indeed N-doped carbons. The high resolution C 1s spectra of NPC samples can be fitted by three peaks with binding energies at around 284.5, 285.2, 286.4 and 288.6 eV (Fig. S7), which were attributed to sp^2 hybridized C-C, C-N, C-O and C=O, respectively.[14] The N 1s core level of NPC-700 (Fig. S6d) were further probed by high-resolution scans, the binding energies around 398.1, 399.1 and 401 eV corresponding to pyridine nitrogen (N-6), pyrrolic/ pyridone (N-5), and quaternary nitrogen (N-Q), respectively.[14a,15] The relative surface concentrations of carbon species obtained by fitting the C 1s and N 1s core level XPS spectra are listed in Table S1. As can be seen that the NPC-600 displays a relatively week sp^2 C-C peeks with lower intensity, indicating amorphous carbon. After annealing at 800 ^{o}C and 900 ^{o}C, the amorphous carbon peeks gradually receded but then the sp^2 peaks displays a sharp shape and increased intensity, suggesting much higher degree of graphitization at increasing pyrolysis temperature. Moreover, It is known that nitrogen doping to porous carbon could enhance the

Journal of Materials Chemistry A Accepted Manuscript

 This journal is © The Royal Society of Chemistry 20xx

wettability and produce the defects in the graphite layer as well as create additional active sites for charge storage,[9e,16] and the quaternary nitrogen (N-Q) in the graphene layers could enhance the electronic conductivity of carbon materials that is important for SCs. It is interesting to note that the quaternary nitrogen (N-Q) was the dominant nitrogen species in all of NPC samples in spite of the contents of the N element gradually decrease with increasing carbonization temperature. The XPS results also confirm that oxygen-containing functional groups exist on the surface of NPC samples. For NPC-700, the O 1s spectrum can be fitted by two peaks located at around 530.9 eV and 532.6 eV (Fig. S8), which are attributed to C=O quinone type groups, C-OH phenol groups and/or C-O-C ether groups.[17] The presence of oxygen functional could participate in faradaic reactions to provide additional pseudocapacitance and the combined effect between nitrogen and oxygen groups was also beneficial for capacitance-enhancement.[14a] Combined with the XPS results, the possible carbon matrices of NPC with the nitrogen and oxygen functionalities are schematically shown in Fig. 2f.

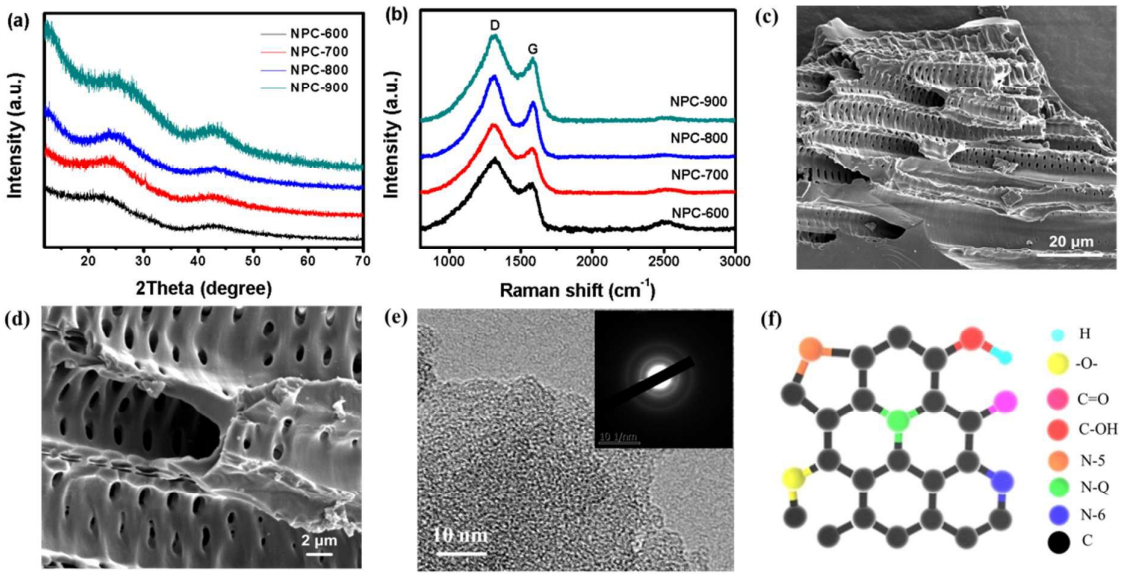

Fig. 2 (a-b) XRD and Raman pattern of NPC-600, NPC-700, NPC-800 and NPC-900, respectively. (c-e) SEM, HRTEM and SAED pattern of the NPC-700. (f) A schematic illustration for the chemical structure of NPC.

High specific capacitance of the electrode materials is highly related to the surface area and its porosity. The porous structure of NPCs samples were investigated by N_2 adsorption-desorption measurements. Type I isotherms with larger slope at lower relative pressures could be found for all the NPC samples, which indicated the existence of substantial micropores (<2 nm) and mesopores (2-50 nm) structures.[9c,14b] The pore size distribution curves confirmed that the NPC samples have micro-mesoporous structures (Fig. S9b). In addition, we also found that the pore volume ratio of micropores *vs.* mesopores and specific surface depend on the carbonization temperature. The porous properties of these materials are summarized in Table S2, it can be seen that the highest surface area (830 $m^2 g^{-1}$) and biggest total pore volume (0.426 $cm^3 g^{-1}$) were obtained in NPC-900, which is comparable to the reported nanoporous carbon materials were prepared by templating, physical or chemical activation method.[18] In comparison, NPC-700 possesses less surface area but the highest fraction of mesopores. For electrochemical double-layer capacitor, the high surface area with abundant micropores is the basic requirement to enables store energy at the electrode/electrolyte interface. On the other hand, the presence of the mesopore also plays a critical role in ion transport and electrolyte diffusion.

In order to test the capacitive activities of NPC electrodes, we measured their electrochemical properties in 6 M KOH aqueous electrolyte in a three-electrode cell with a saturated calomel electrode (SCE) as reference electrode and a Pt counter-electrode. For comparison, porous carbon without nitrogen (PC-700) and Ni foam (NF) electrode was also measured. Cyclic voltammetry (CV) curves of NPC-700, PC-700 and NF electrodes collected 20 mV s^{-1} are shown in Fig. 3a. Compared with NPC-700 and PC-700 electrodes, the NF electrode shows much little current density, indicating that NF has a very weak contribution for electrochemical capacitance of NPC and PC electrodes. The NPC-700 electrode shows a much higher current density than that PC-700 electrode with a similar mass loading (1 mg cm^{-2}), indicating that the substantial enhancement of capacitance activity was due to doped heteroatom (N). The rectangular shape of the CV curves of NPC-700 electrode is the characteristic of double-layer capacitor (Fig. 3b). Significantly, the CV profiles still remain rectangularly shape even when the scan rate increases from 1 to 100 mV s^{-1} demonstrating its excellent rate capability and capacitive behavior. Furthermore, in comparison to CV curves of the NPC-600, NPC-800 and NPC-900, the NPC-700 electrode also exhibits higher current density (Fig. S10). The electrochemical performance of NPC electrodes were further studied by galvanostatic charge-discharge (GCD) measurements. Fig. 3c displays the GCD curves of NPC-700 electrode collected at various current densities. The maximum discharge time (Fig. S11) and the

Journal of Materials Chemistry A Accepted Manuscript

minimum iR drop (0.006 V, Fig. S12) of the NPC-700 electrode reveal its optimal capacitance and superior conductivity. Additionally, compared to the un-doped PC-700 electrode, longer discharge time and more symmetrical GCD curves are observed for the NPC electrodes, indicating the enhanced capacitance and superior coulombic efficiency of the NPC electrodes. The superior conductivity of the NPC electrodes was further confirmed by electrochemical impedance spectroscopy. As shown in Nyquist plots (Fig. 3d), all the curves of the NPC electrodes are showing a rapid upward trend in the low-frequenc region, indicating a good capacitive behavior. The corresponding equivalent circuit diagram (Fig 3d inset; R1: equivalent series resistance, R2: charge transfer resistance of NPC, R3: charge transfer resistance of Ni foam, CPE1: double layer capacitance of NPC, CPE2: double layer capacitance of Ni foam, and Zw: Warburg impedance) indicates that the charge-transfer resistance (Table S4) of the NPC-700 electrode is smaller than other NPC electrodes. Since the NF electrode has only weak contribution to the capacitance of the NPC electrodes, its influence can be ignored in this work. Fig. 3e compares the specific capacitance and rate performance of the NPC electrodes (for detailed calculation see supporting information). As expected, the highest specific capacitance of 321.7 F g^{-1} was obtained for NPC-700 electrode at a current density of 1 A g^{-1} and good rate capability (51.4% of the initial capacitance at 20 A g^{-1}), which is higher than the previously reported carbon electrodes derived from other biomass wastes (Table S4) and other carbon nanostructured electrodes, such as 3D hierarchical porous carbon (318.2 F g^{-1} at 0.5 A g^{-1}),[17] Graphene hydrogel film (196 F g^{-1} at 0.5 A g^{-1}),[19] Mesoporous Graphene Nanoballs (206 F g^{-1} at 5 mV s^{-1}),[20] Nitrogen-Doped Porous Carbon Nanofibers (202 F g^{-1} at 1 A g^{-1}).[21] The significantly enhanced electrochemical of NPC-700 electrode can be due to the following reasons: 1) the nitrogen doping and fractional graphitization in porous carbon can enhance the electrical conductivity; 2) abundant micropores in carbon materials provide a high surface area; 3) the mesopores constructs in the carbon materials facilitate electrolyte accessibility to the microporous area and serving as ion-transport pathways enhanced rapid ion transport. The long-term cycling stability of NPC-700 electrode was evaluated by CV test at a high scan rate of 200 mV s^{-1}. As shown in Fig. 3f, there is a slow increase during the first initial 5000 cycles which is probably due to the slow activation process of electroactive material during the charge/discharge process at a high scan rate. After that, there is no capacity decay observed over 20 000 cycles indicates remarkable electrochemical stability. These results convincingly show that the as-prepared NPC-700 electrode suitable for a high performance negative electrode for ASCs.

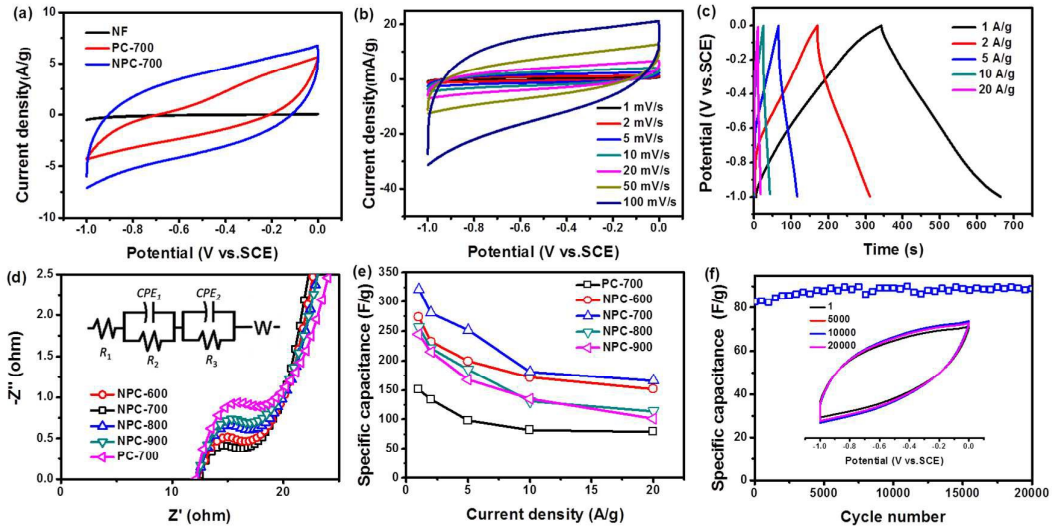

Fig. 3 (a) CV curves of Ni foam, PC-700 and NPC-700 electrodes at a scan rate of 20 mV s^{-1}. (b) CV curves of NPC-700 electrode at scan rates of 1-100 mV s^{-1}. (c) GCD curves of NPC-700 electrode at different current densities of 1-20 A g^{-1}. (d) Nyquist plots of the PC-700 and NPC electrodes (Inset: the corresponding equivalent circuit diagram). (e) Specific capacitance of PC-700 and NPC electrodes calculated from GCD curves as a function of current density. (f) Cycling performance of NPC-700 electrode collected at a scan rate of 200 mV s^{-1} for 20 000 cycles (Inset: representative CV curves collected initially and at the 1, 3,000, 6,000 and 9,000 cycles).

To test the practical application of the NPC-700 as a negative electrode for SCs device, a solid-state ASC device using MnO_2 and NPC-700 as the positive and negative electrode was assembled as shown in Fig. 4a (denoted as MnO_2//NPC-ASC). MnO_2 was used as the positive electrode because of its outstanding capacitive performance, simple synthesis, and wide voltage window than Ni, Co based oxide.[22] Hence, MnO_2 was uniformly grown on Ni foam using an electrodeposition approach (Fig. S13). Typical Mn 2p spectrum with peak binding energy separation (12.2 eV) between Mn $2p_{3/2}$ and Mn $2p_{1/2}$ was confirming the presence of α-MnO_2 (Fig. S14).[23] To obtained the maximize performance of the MnO_2//NPC-ASC device, the charge between the NPC-700 and MnO_2 electrodes should be balanced. The mass ratio of the NPC-700 to MnO_2 was calculated to be about 1.25:1 (for details, see the Supporting Information and Fig. S15). Fig. 4b show the CV curves of the optimized MnO_2//NPC-ASC device collected at different voltage windows, the stable voltage window of the device can be extended to 1.8 V. Moreover, the as-prepared

This journal is © The Royal Society of Chemistry 20xx

Journal of Materials Chemistry A Accepted Manuscript

devices display outstanding flexibility and mechanical properties under severe bending state with almost the same of electrochemical performance (Fig. 4c). The GCD curves of the MnO_2//NPC-ASC device measured at various current densities exhibit relatively symmetric shapes, indicating its superior capacitive behavior (Fig. S16a). Fig. 4d present the calculated specific capacitance (based on the total mass of active material) of the MnO_2//NPC-ASC device as a function of current densities based on the GCD curves. A maximal specific capacitance (182.5 F g^{-1}) of the device was achieved at a current density of 1 A g^{-1}. Additionally, a remarkable rate capacitance also has been achieved, with 63% of the initial capacitance retained even when the current density increases to 20 A g^{-1}. In order to investigate the long-term cycling stability of the as-assemble MnO_2//NPC-ASC device under distortion situations, GCD studies were performed under normal, bent and fold state., There is no obvious decrease after 2000 cycles under normal state as shown in Fig. 4e. After that, the MnO_2//NPC-ASC device was continuously tested for further 2000 cycles under the bent and fold state, respectively. Only a 6.6% reduction of the initial capacitance after 6000 cycles, the loss of the capacitance due to the structural broken of Ni foam substrate under drastic distortion.

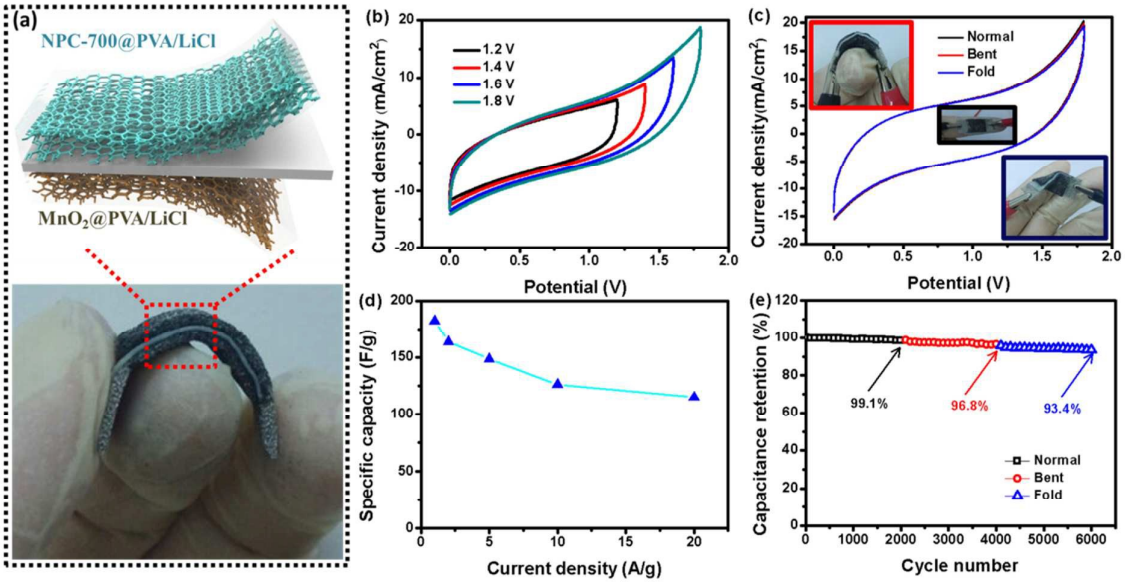

Fig. 4 (a) Optical photograph and a schematic diagram of the fabricated MnO_2//NPC-700 ASC device. (b) CV curves of the MnO_2//NPC-700 ASC device collected in different scan voltage windows. (c) CV test at different bent states at 200 mV s^{-1}. (d) Specific capacitance of MnO_2//NPC-700 ASC device calculated from GCD curves as a function of current density. (e) Cycling performance of MnO_2//NPC-700 ASC device at different bending states for 20 000 cycles.

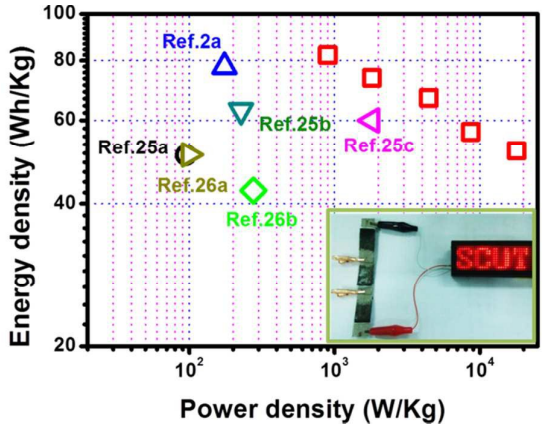

Fig. 5 Ragone plots of the MnO_2//NPC-700 ASC device. Inset: A LED powered by three MnO_2//NPC-700 ASC devices in series.

The energy density (*E*) and power density (*P*) are two important parameters to evaluate the electrochemical performance of SCs. Fig. 5 compares the energy and power densities of MnO_2//NPC-ASC device to some other recently reported Carbon based ASCs. Notably, our MnO_2//NPC-ASC device shows an average power density of 900 W Kg^{-1} and a remarkable energy density of 82.1 W h Kg^{-1} at a current density of 1 A g^{-1}. This value is comparable to the activated carbon (derived from pollens)-based SSC in ionic liquid electrolytes (88 W h Kg^{-1}),[24] and substantially higher than recently reported carbon based ASCs device,[2a,25] such as $Ni(OH)_2$/Graphene//porous graphene-ASCs (77.8 W h Kg^{-1}), $Ni(OH)_2$/CNT//AC-ASCs (50.6 W h Kg^{-1}), CBP/MnO_2//a-CBP-ASCs (63 W h Kg^{-1}), Co-Ni-S// porous graphene-ASCs (60 W h Kg^{-1}). Significantly, this present energy density is also higher than those reported oxide based ASCs,[26] such as MnO_2/FGS//Fe_2O_3/FGS-ASCs (50.7 W h Kg^{-1}), RGO/MnO_2// RGO/MoO_3-ASCs (42.6 W h Kg^{-1}). To demonstrate the practical application of our as-prepared solid-state MnO_2//NPC-ASC device, we connected the device units in series to power red light-emitting diodes (LED, 3.5V). These tandem devices (two or three units in series) exhibit an enhanced voltage window with changeless discharge time (Fig. S16b). Here, a LED with red "SCUT" logo can be powered by three tandem devices (the inset in Fig. 5) for more than 1 min after charging for 20 s at current density of 10 A g^{-1}.

Journal of Materials Chemistry A Accepted Manuscript

Conclusions

In summary, a scalable and smart approach was developed to transform the crude biomass waste (shaddock peels) into N-doped porous carbon without template or pretreatment process as high performance negative electrode for ASCs application. The as-obtained NPC with high surface area, high hierarchical porosity and high N-doping exhibit a remarkable capacitance of 321.7 F g^{-1} at a current density of 1 A g^{-1}, as well as excellent long-term cycling stability without obvious decay of capacitance after 20000 cycles. Additionally, a high-performance ASC device based on the as-prepared NPC-700 as the negative electrodes and MnO_2 as positive electrodes was also prepared. The MnO_2//NPC-700 ASC device delivered a maximum energy density of 82.1 W h Kg^{-1} at a current density of 1 A g^{-1}, which is much higher than those of most reported carbon-based ASCs and SSCs. Besides large energy density, The MnO_2//NPC-700 ASC device also exhibits excellent stability (only 6.6% capacitance loss after 6000 cycles under bending state). This work shows a promising strategy to synthesize porous carbon as a high-performance negative electrode for high energy density ASCs.

Acknowledgements

This study was supported by the National Science Fund for Distinguished Young Scholars of China (no. 21225625), National Natural Science Foundation of China (21406078), the Pearl River Scholar Program of the Guangdong Province and the Fundamental Research Funds for the Central Universities.

Notes and references

1 (a) Y. Gogotsi, P. Simon, *Science*, 2011, **334**, 917; (b) M. Armand, J. M. Tarascon, *Nature*, 2008, **451**, 652; (c) Z. G. Yang, J. L. Zhang, M. C. W. Kintner-Meyer, X. C. Lu, D. W. Choi, J. P. Lemmon, J. Liu, *Chem. Rev.*, 2011, **111**, 3577; (d) C. G. Liu, Z. N. Yu, D. Neff, A. Zhamu, B. Z. Jang, *Nano Lett.*, 2010, **10**, 4863.

2 (a) J. Yan, Z. J. Fan, W. Sun, G. Q. Ning, T. Wei, Q. Zhang, R. F. Zhang, L. J. Zhi, F. Wei, *Adv. Funct. Mater.*, 2012, **22**, 2632; (b) X. H. Lu, T. Zhai, X. H. Zhang, Y. Q. Shen, L. Y. Yuan, B. Hu, L. Gong, J. Chen, Y. H. Gao, J. Zhou, Y. X. Tong, Z. L. Wang, *Adv. Mater.*, 2012, **24**, 938; (c) X. H. Lu, M. H. Yu, G. M. Wang, Y. X. Tong, Y. Li, *Energy Environ. Sci.*, 2014, **7**, 2160.

3 (a) L. Y. Yuan, X. H. Lu, X. Xiao, T. Zhai, J. J. Dai, F. C. Zhang, B. Hu, X. Wang, L. Gong, J. Chen, C. G. Hu, Y. X. Tong, J. Zhou, Z. L. Wang, *ACS Nano* **2012**, *6*, 656.; (b) G. P. Wang, L. Zhang, J. J. Zhang, *Chem. Soc. Rev.* **2012**, *41* 797.; (c) Y. Z. Su, K. Xiao, N. Li, Z. Q. Liu, S. Z. Qiao, *J. Mater. Chem. A* **2014**, *2*, 13845.

4 (a) G. F. Chen, Z. Q. Liu, J. M. Lin, N. Li, Y. Z. Su, *J. Power Sources*, 2015, **283**, 484; (b) G. F. Chen, Y. Z. Su, P. Y. Kuang, Z. Q. Liu, D. Y. Chen, X. Wu, N. Li, S, Z. Qiao, *Chem. Eur. J.*, 2015, **21**, 4614.

5 M. F. El-Kady, V. Strong, S. Dubin, R. B. Kaner, *Science*, 2012, **335**, 1326.

6 (a) M. F. L. DeVolder, S. H. Tawfick, R. H. Baughman, A. J. Hart, *Science*, 2013, **339**, 535; (b) S. Park, M. Vosguerichian, Z. A. Bao, *Nanoscale*, 2013, **5**, 1727.

7 L. L. Zhang, X. S. Zhao, *Chem. Soc. Rev.*, 2009, **38**, 2520.

8 (a) Z. J. Fan, J. Yan, T. Wei, L. J. Zhi, G. Q. Ning, T. Y. Li, F. Wei, *Adv. Funct. Mater.*, 2011, **21**, 2366; (b) S. J. Peng, L. L. Li, H. B. Wu, S. Madhavi, X. W. Lou, *Adv. Energy Mater.*, 2014, DOI: 10.1002/aenm.201401172; (c) X. Wang, C. Y. Yan, A. Sumboja, P. S. Lee, *Nano Energy*, 2013, **3**, 119; (d) R. R. Salunkhe, J. J. Lin, V. Malgras. S. X. Dou, J. H. Kim, Y. Yamauchi, *Nano Energy*, 2015, **11**, 211.

9 (a) E. M. Lotfabad, J. Ding, K. Cui, A. Kohandehghan, W. P. Kalisvaart, M. Hazelton, D. Mitlin, *ACS Nano*, 2014, **8**, 7115; (b) J. Ding, H. L. Wang, Z. Li, K. Cui, D. Karpuzov, X. H. Tan, A. Kohandehghan, D. Mitlin, *Energy Environ. Sci.*, 2015, **8**, 941; (c) J. Jiang, J. H. Zhu, W. Ai, Z. X. Fan, X. N. Shen, C. J. Zou, J. P. Liu, H. Zhang, T. Yu, *Energy Environ. Sci.*, 2014, **7**, 2670; (d) P. Chen, L. K. Wang, G. Wang, M. R. Gao, J. Ge, W. J. Yuan, Y. H. Shen, A. J. Xie, S. H. Yu, *Energy Environ. Sci.*, 2014, **7**, 4095; (e) H. W. Wang, H. Yi, C. R. Zhu, X. F. Wang, H. J. Fan, *Nano Energy*, 2015, **13**, 658; (f) E. Redondo, J. Carretero-González, E. Goikolea, J. Ségalini, R. Mysyk, *Electrochim. Acta*, 2015, **160**, 178; (g) M. Genovese, J. H. Jiang, K. Lian, N. Holm, *J. Mater. Chem. A*, 2015, **3**, 2903.

10 C. L. Long, X. Chen, L. L. Jiang, L. J. Zhi, Z. J. Fan, *Nano Energy*, 2015, **12**, 141.

11 J. Hou, C. Cao, F. Idrees, B. Xu, X. Hao, W. Lin, *Sci. Rep.*, 2014, **4**, 7260.

12 J. H. Hou, C. B. Cao, F. Idrees, X. L. Ma, *ACS Nano*, 2015, **9**, 2556.

13 S. Y. Gao, K. Geng, H. Y. Liu, X. J. Wei, M. Zhang, P. Wang, J. J. Wang, *Energy Environ. Sci.*, 2015, **8**, 221.

14 (a) D. Hulicova-Jurcakova, M. Seredych, G. Q. Lu, T. J. Bandosz, *Adv. Funct. Mater.*, 2009, **19**, 438; (b) J. K. Ou, Y. Z. Zhang, L. Chen, Q. Zhao, Y. Meng, Y. Guo, D. Xiao, *J. Mater. Chem. A*, 2015, **3**, 6534.

15 W. H. Shin, H. M. Jeong, B. G. Kim, J. K. Kang, J. W. Choi, *Nano Lett.*, 2012, **12**, 2283.

16 Z. Li, Z. W. Xu, X. H. Tan, H. L. Wang, C. M. B. Holt, T. Stephenson, B. C. Olsen, D. Mitlin, *Energy Environ. Sci.*, 2013, **6**, 871.

17 L. Qie, W. M. Chen, H. H. Xu, X. Q. Xiong, Y. Jiang, F. Zou, X. L. Hu, Y. Xin, Z. L. Zhang, Y. H. Huang, *Energy Environ. Sci.*, 2013, **6**, 2497.

18 (a) G. P. Mane, S. N. Talapaneni, C. Anand, S. Varghese, H. Iwai, Q. M. Ji, K. Ariga, T. Mori, A. Vinu, *Adv. Funct. Mater.*, 2012, **22**, 3596; (b) Y. S. Hu, P. Adelhelm, B. M. Smarsly, S. Hore, M. Antonietti, J. Maier, *Adv. Funct. Mater.*, 2007, **17**, 1873; (c) D. D. Li, L. X. Ding, H. B. Chen, S. Q. Wang, Z. Li, M. Zhu, H. H. Wang, *J. Mater. Chem. A*, 2014, **2**, 16617.

19 Y. X. Xu, Z. Y. Lin, X. Q. Huang, Y. Liu, Y. Huang, X. F. Duan, *ACS Nano*, 2013, **7**, 4042.

20 J. S. Lee, S. I. Kim, J. C. Yoon, J. H. Jang, *ACS Nano*, 2013, **7**, 6047.

21 L. F. Chen, X. D. Zhang, H. W. Liang, M. G. Kong, Q. F. Guan, P. Chen, Z. Y. Wu, S. H. Yu, *ACS Nano*, 2012, **6**, 7092.

Journal of Materials Chemistry A Accepted Manuscript

This journal is © The Royal Society of Chemistry 20xx

22 X. H. Lu, D. Z. Zheng, T. Zhai, Z. Q. Liu, Y. Y. Huang, S. L. Xie, Y. X. Tong, *Energy Environ. Sci.*, 2011, **4**, 2915.
23 K. Xiao, J. W. Li, G. F. Chen, Z. Q. Liu, N. Li, Y. Z. Su, *Electrochim. Acta*, 2014, **149**, 341.
24 L. Zhang, F. Zhang, X. Yang, K. Leng, Y. Huang, Y. S. Chen, *Small*, 2013, **9** 1342.
25 (a) Z. Tang, C. H. Tang, H. Gong, *Adv. Funct. Mater.*, 2012, **22**, 1272; (b) C. L. Long, D. P. Qi, T. Wei, J. Yan, L. L. Jiang, Z. J. Fan, *Adv. Funct. Mater.*, 2014, **24**, 3953; (c) W. Chen, C. Xia, H. N. Alshareef, *ACS Nano*, 2014, **8**, 9531.
26 (a) H. Xia, C. Y. Hong, B. Li, B. Zhao, Z. X. Lin, M. B. Zheng, S. V. Savilov, S. M. Aldoshin, *Adv. Funct. Mater.*, 2015, **25**, 627; (b) J. Chang, M. Jin, F. Yao, T. H. Kim, V. T. Le, H. Yue, F. Gunes, B. Li, A. Ghosh, S. Xie, Y. H. Lee, *Adv. Funct. Mater.*, 2013, **23**, 5074.

Journal of Materials Chemistry A Accepted Manuscript

Journal Name

ARTICLE

Graphical Abstract

Nitrogen-doped Porous Carbon Derived from Residuary Shaddock Peels: A Promising and Sustainable Anode for High Energy Density Asymmetric Supercapacitors†

Kang Xiao,[a] Liang-Xin Ding,*[a] Hongbin Chen,[a] Suqing Wang,[a] Xihong Lu[b] and Haihui Wang*[a]

Here we introduce a scalable and smart strategy to convert the crude biomass waste (shaddock peels) into high quality porous carbon and successfully use it as the high-performance and sustainable electrode material for high energy density asymmetric supercapacitors.

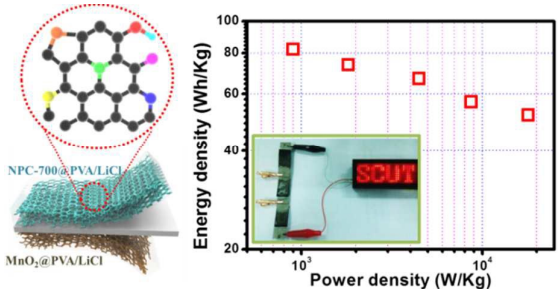

Journal of Materials Chemistry A Accepted Manuscript